Low Temperature Physics/Fizika Nizkikh Temperatur, 2012, v. 38, No. 8, pp. 942–948

Inner valence excitations of condensed neon

B. Kassühlke* and P. Feulner

Physikdepartment E20, TU-München, D-85748 Garching, Germany
E-mail: feulner@tum.de

Received April 6, 2012

Applying two-dimensional electron spectroscopy, we investigate bound and continuum excitations of neon films condensed onto clean metal surfaces, in the energy range of the [Ne 2*s*] singly and [Ne $2p^2$] doubly excited states. Precise energy values of excitons and ionization potentials are obtained for the surface and for the bulk, and compared to data for the isolated neon atom. In addition, valuable information on the mobility and the decay of excitons in this energy range is accessible with our technique.

PACS: **73.20.–r** Electron states at surfaces and interfaces;
73.20.At Surface states, band structure, electron density of states;
73.21.Ac Multilayers.

Keywords: condensed neon, surface and bulk excitations, excitons decay.

Introduction

Solid neon is the insulator with the largest band gap that crystallizes at ambient pressure and below [1], and calculations show that it will become metallic only under extreme conditions [2]. Opposed to solidified He, its zero point energy is still small compared to interatomic attraction and quantum effects are not very prominent, although not negligible [3]. For this light element of the second row of the periodic table, LS coupling is a good description for the excitation energy range investigated here [4], in contrast to the heavier rare-gas atoms. The oscillator strengths of LS forbidden transitions are small for Ne in this photon energy range [5]. This fact, and its closed shell nature result in an electronic excitation spectrum that is not too complicated, even for multiply excited states [4]. Ne is therefore an ideal model system for the investigation of singly and multiply excited Rydberg states derived from closed shell entities with occupied *s* and *p* levels.

Because of this model character, Ne is well suited for the study of condensation effects like i) the transformation of Rydberg states into excitons with different levels of mobility [6]; ii) the interaction of the exited electron(s) with the ground state neighbors in the surrounding matrix, e.g., caging of the wave functions by Pauli repulsion and polarization screening — commonly these two effects result in a compression of Rydberg series and a shift of their series limits [1,6,7]; iii) effects that are induced by the symmetry breaking at the surface of the solid, i.e., differences of surface and bulk excitations [1,6,7]; iv) condensation induced changes of the electronic decay channels [8]; and finally v) biexcitonic effects [9]. Any electronic excitation of Ne creates an open shell system and therefore destroys the chemical inertness of this material.

Unfortunately, solid neon is not the easiest material for studies of electronic properties, in particular if surface effects have to be included. Whereas optical methods are perfect for investigations of bulk properties [10], surface studies require strongly interacting probes. As such, electrons, ions or particles in metastable electronic states are well suited [7]. Among these possibilities, electron spectroscopy in combination with tuneable synchrotron radiation is the method that promises the most detailed information. Other boundary conditions of the experiment as a sample temperature of not more than 6 K and a perfect ultra high vacuum (UHV) in the 10^{-11} mbar range are implied by the low heat of solidification of Ne [1,6,11] and by the purity requirement of surface experiments.

Electronic excitations of Ne comprise three different energy regions: the outer valence range of singly excited 2*p* levels around 20 eV [1,4,6,7], the 2*s* inner valence region including $2p^2$ and 2*s*2*p* double excitations above 45 eV [4,12,23,24], and finally the Ne 1*s* core level regime above the 1*s* threshold at 868.3 eV for the solid [7,8,13,14]. In previous experiments we have studied all of these energy ranges [7–9,12–14], the region of 2*s* single and $2p^2$ double ionization however only by recording desorbing ions and rather poorly resolved total electron yield

* Present address: BMW Group, FZ-430, ERP Service and Operations, 80788 München, Germany

(TEY) spectra [12], mainly because of experimental limitations. To improve and extend the data of this energy range is the focus of the present study. By applying two-dimensional (2D) electron spectroscopy [15], we are able to obtain a detailed picture of neutral and ionic excitations in this range as well as information on their mobility and electronic decay.

Experiment

We performed the measurements at the synchrotron radiation source BESSY in Berlin (single bunch operation) in an UHV apparatus with a base pressure in the 10^{-11} mbar range. Our samples were Ne films condensed onto a monocrystalline Ru(001) substrate. Before dosing the Ne films, the Ru substrate was cleaned by sputtering with Ar ions, repeated heating in 10^{-6} mbar of O_2, and final flashing to 1570 K for 60 s. Its cleanliness was check by XPS. The Ne films were dosed onto the substrate that was cooled below 6 K with a liquid He flow cryostat. The gas doser was equipped with a microchannel array for a spatially homogeneous gas flux. The (homogeneous) thickness of the layers was calibrated by thermal desorption spectroscopy [11]. After dosing and before data acquisition with synchrotron radiation, the Ne layers were annealed close to the onset of multilayer desorption. This was necessary to minimize electron emission at the vacuum level which was found to be indicative of scattering by defects [16]. For maximum surface sensitivity, the sample was illuminated under grazing incidence. The **E** vector of the light was tilted with respect to the surface normal by 7° (A_z polarization). Emitted electrons were detected with a time-of-flight spectrometer in combination with a time-to-digital converter. In the next step we converted the data from the time-of-flight to the kinetic energy domain, thereby correcting for different channel (= bin) sizes in the two representations, and for angle effects. The data have also been normalized to the photon flux obtained either from the photocurrent of the refocusing mirror of the monochromator, or from the photocurrent of a highly transparent gold grid inserted into the beam. Mirror and grid current served as secondary calibration sources; as a primary standard for the calibration of their yield functions we used the ion yield of neon gas. Absorption maxima in the gas signal served also as calibration points for the photon energy scale. Great care was taken to avoid charging especially of the thicker Ne layer by continuously scanning the beam over the sample surface during data acquisition. In addition, structural defects and contaminants at the surface, which both favor charging, have been minimized by careful annealing and good vacuum (see above).

Results and discussion

We obtained 2D spectra by recording dense data fields in the plane with the axes "photon energy" and "kinetic energy" [15]. Figure 1 shows such a spectrum from a well-annealed Ne multilayer.

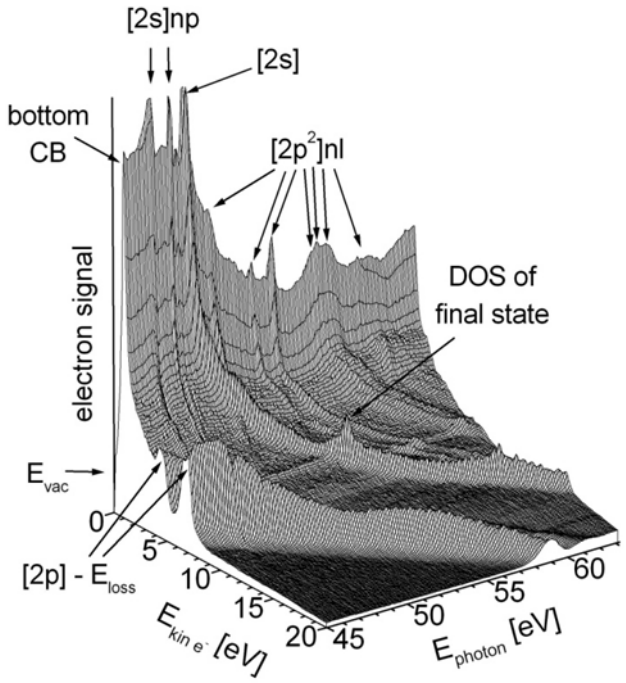

Fig. 1. Two-dimensional spectrum of the [Ne 2*s*] single and [Ne $2p^2$] double excitation region from a 25 layers thick Ne film on Ru(001) (see text for details).

Compared to common 1D photoemission spectroscopy, the gain of information is enormous. Different classes of excitations are clearly discernible, allowing assignments of their nature simply by their shape. The electron signal's cut-off at low kinetic energy defines the vacuum level E_{vac} (and is a perfect calibration mark for the zero point of the kinetic energy scale; as calibration point for the upper end of the E_{kin} scale we used the signal of the stray light that was also recorded with our TOF set up). The large signal at E_{kin} = 1 eV denotes the bottom of the conduction band. Solid Ne has negative electron affinity, i.e., the bottom of the conduction band E_{cb} lies above E_{vac} and most secondary electrons are therefore emitted hot (Fig. 1). We note that our value for the electron affinity of –1 eV (independent of film thickness for 10 layers and more) is slightly lower than that reported previously [1]. We think, however, that our value is correct because i) our energies for outer valence excitons agree perfectly with optical data [1,6], and because ii) all of these exciton energies (see below) and the value for the negative electron affinity are extracted from identical data sets, for which a calibration error of 30% of the E_{kin} scale for the 1 eV interval between E_{vac} and E_{cb} can safely be excluded. Excitation of ionic states gives rise to constant initial state (CIS) features that appear as diagonal traces over the E_{kin}/E_{photon} plane. The [2*s*] emission and some [$2p^2$]*nl* ionization satellite lines can be discerned. The CIS patterns in the foreground of Fig. 1 belong to extrinsic loss satellites of the [2*p*] emis-

sion, one at a loss energy of 17.5 eV and the second at 19.75 eV. The first loss energy coincides with the excitation energy of the $n = 1$ bulk exciton that has $[2p]3s$ character [1,6,7]. The second one has no such counterpart in optical excitation spectroscopy. We explain it by the $[2p]3p$ transition that is optically dipole forbidden but can be excited with slow electrons.

All of these CIS traces show intensity modulation as a function of E_{kin} and E_{photon}. Some extrema are of minor state selectivity, i.e., they appear in nearly all traces at identical E_{kin} values, e.g., the maxima at $E_{\text{kin}} \sim 7$ eV. At this energy, the secondary electron background is also maximal at all photon energies. Such an enhancement in nearly all channels is due to a large density of states in the unoccupied bands of solid Ne [17]. Other (smaller) extrema show up at photon energies for which CIS traces cross the signatures of neutral excited states. They indicate autoionization of neutral into ionic states; examples for such process will be discussed below.

In optical spectroscopy, excitations of neutral states are commonly investigated by recording, as a function of E_{photon}, either the attenuation of the transmitted beam, or the fluorescence photons emitted upon excitation decay. In our experiment we measure photoabsorption by acquiring the total electron yield (TEY) as a function of E_{photon}. This is a standard method in inner shell spectroscopy of solid samples [18]; its application is justified here as well because most neutral excitation in thin rare-gas solid films on metals will decay nonradiatively [19], in particular for our energy range. In Fig. 1, neutral excitations (or excitons) appear as traces at constant E_{photon} that cut the diagonal CIS features, best seen for the $[2s]np$ excitations and a few $[2p^2]nl, n'l'$ doubly excited states.

In order to extract information on different types of electronic excitations we reduce our 2D spectra to 1D data sets (Fig. 2) in specific ways. TEY spectra for the identification of neutral states are obtained by integrating over E_{kin} (Fig. 2,*a*,*b*). Depending on the thickness of the layer, either bulk (*a*) or surface excitations prevail (*b*). Signatures of ionic states are visible in the electron signals at distinct kinetic energies as a function of $h\nu$: ionization of surface states (= outer ionization) is best seen in the threshold electron signal (Fig. 2,*c*), whereas values for ionization potentials of the bulk (= inner ionization) are obtained from the electrons with kinetic energies corresponding to the bottom of the conduction band (Fig. 2,*d*).

The most prominent features in these spectra are the members of the bulk and surface $[2s]np$ Rydberg series converging to the $[2s]$ limits at 48.9 and 47.9 eV for the bulk and the surface, respectively (see Table 1 for a compilation of all excitation energies). The energetic positions of the series limits are easily extracted from the electron spectra in Fig. 2,*c*,*d*; for the determination of the exciton energies, however, fitting of the data to a Fano profile is necessary because of their bipolar line shapes (see, e.g., the peak

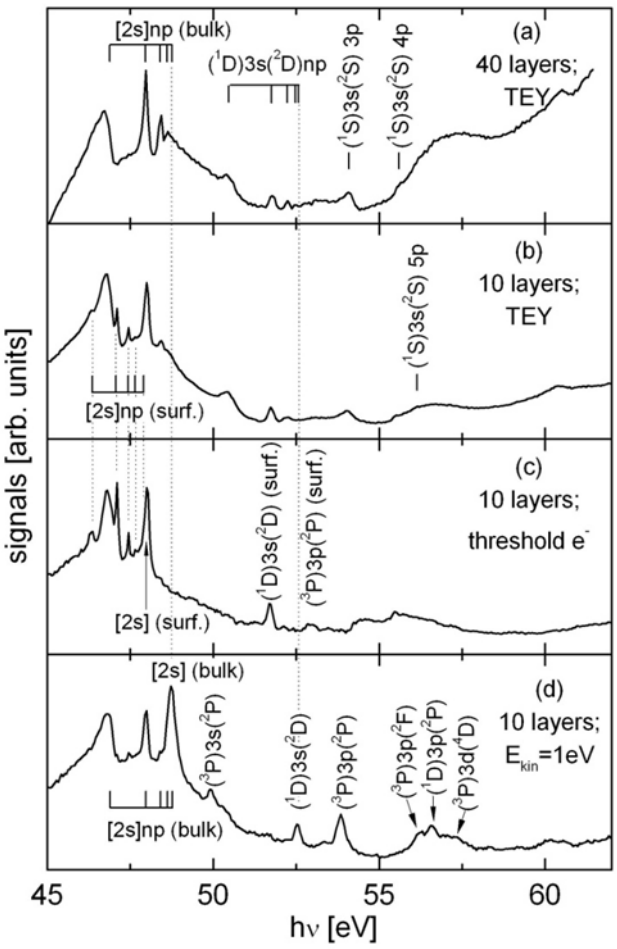

Fig. 2. 1D spectra extracted from 2D data sets as shown in Fig. 1. TEY spectra show maxima at neutral bulk (*a*) and surface excitations (*b*). The threshold electron signal ($0 \le E_{\text{kin}} \le 10$ meV) indicates ionic surface states (outer ionization, (*c*)), the electron yield at E_{kin} corresponding to the bottom of the conduction band indicates production of free electrons inside the solid (inner ionization potential (*d*)).

belonging to the $[2s]3p$ bulk excitation in Fig. 2,*a*). Fano profiles arise from interaction of bound resonant states with one or more continua [20]. For the isolated atom [4], the $[2s]np$ neutral states interact with the $[2p]$ continuum in which they decay by autoionization. According to the Fano formula, the shape of such a photoabsorption resonance is described by the excitation cross section σ as a function of de-tuning ε, normalized to the resonance width Γ:

$$\sigma(\varepsilon) = \sigma_a (q-\varepsilon)^2/(1+\varepsilon^2) + \sigma_b; \;\; \varepsilon = (h\nu - h\nu_{\text{res}})/(\Gamma/2);$$

q is a line shape parameter with the value of –1.6 for Ne gas [4], and σ_a and σ_b denote the cross sections of the continua that do and do not interact with the resonant state, respectively [20]. Applying this formula to our $[2s]3p$ data we obtain q values between –1.55 and –1.63 for different data sets which within the experimental scatter agree with the value for the isolated Ne atom. For the resonance ener-

gy (bulk) we obtain 46.85 eV and for the width 290 meV, i.e., less than the value of 340–360 meV from previous optical absorption measurements [10], but much more than for Ne in the gas phase (Γ = 13 meV [4]). Obviously, a condensation induced broadening effect comes into play that cannot simply be explained by lifetime broadening. Comparing the widths of the [2*s*]3*p* and [1*s*]3*p* excitons [13], we find after deconvolution of experimental broadenings and of the natural lifetime width of the [1*s*] core hole of 240 meV [21] practically identical resonance widths of ~300 meV for the [1*s*]3*p* and the [2*s*]3*p* states. This result indicates that condensation induced broadening is due to the interaction of the excited electron in the 3*p* orbital with the surrounding matrix for both edges. The holes are of minor importance despite the large binding energy difference between [2*s*] and [1*s*], which also corresponds to different orbitals sizes. These hole orbitals, however, are both small compared to the 3*p* wave function. We note that gas phase [2*s*]3*p* Fano profiles convoluted with a 300 meV broad Gaussian mimick perfectly our experimentally obtained [2*s*]3*p* line profile.

In our previous study of [1*s*]*np* core excitons [13] we found the resonance line belonging to the [1*s*]3*p* state to be considerably broader than those of the [1*s*]4*p* and [1*s*]5*p* excitations, an effect that is observed here for the [2*s*]*np* series as well, for the bulk as well for the surface states (Fig. 2,*a*,*b*). For the [1*s*]*np* series, this was tentatively explained by the different sizes of the *np* states: 3*p* is relatively small and caged by the neighboring atoms, i.e., its energy is sensitive to its actual position inside the cage. It feels inhomogeneities of the crystal structure as well as thermally stimulated and zero point motions relative to the surrounding atoms, opposed to 4*p* and 5*p* which extend over several unit cells of the Ne lattice, thus averaging over displacements of individual atoms. This speculative explanation was corroborated by theory, which showed that the 3*p* orbital is compressed by condensation and caged, whereas 4*p* and 5*p* are expanded with respect to the isolated atom by screening [22]. The present data show that identical effects exist for the [N 2*s*]*np* region.

At and above the [2*s*] excitation range neutral and ionic states with two holes in the 2*p* shell are observed (Fig. 2). LS coupling allows three different doubly ionized Ne^{++} cores with $1s^2 2s^2 2p^4$ configuration, namely ^3P, ^1D and ^1S [4], also known as final states of [1*s*] Auger decay [8]. By adding an electron in an n = 3 orbital to these cores, the configurations of the lowest and most intense satellites to [2*p*] photoemission are obtained (Fig. 2,*c*,*d*). Doubly excited Rydberg series of $1s^2 2s^2 2p^4 nl, n'l'$ configuration converge towards these limits (Fig. 2,*a*,*b*), the $(^1D)3s(^2D)np$ and $(^1S)3s(^2S)np$ series are the most intense (Fig. 2,*a*,*b*). Spectra from very thin layers also show the $(^3P)3s(^2P)3p$ (surface-) state that lies, as for the gas phase, even below the lowest [2*s*]*np* excitation (Table 1).

Table 1. Excitation energies of neutral and ionic surface and bulk states of condensed Ne (in eV), Values for the isolated atom (from Refs. 4, 23, 24) are given for comparison, as well as the condensation shifts (tentative values in parenthesis). The value denoted by an asterisk was obtained from a very thin film (~ 3 monolayers thick).

State	$E_{surface}$	E_{bulk}	E_{gas}	$\Delta E_{bulk-gas}$
Neutral states				
$2p^4(^3P)3s(^2P)3p(^1P)$	45.50*		44.98	
$2s^1 2p^6(^2S_{1/2})3p(^1P)$	46.32	46.85	45.55	1.30
$2s^1 2p^6(^2S_{1/2})4p(^1P)$	47.11	48.00	47.12	0.88
$2s^1 2p^6(^2S_{1/2})5p(^1P)$	47.45	48.44	47.69	0.75
$2s^1 2p^6(^2S_{1/2})6p(^1P)$	47.65	48.70	47.97	0.73
$2p^4(^1D)3s(^2D)3p(^1P)$		50.40	48.91	1.49
$2p^4(^1D)3s(^2D)4p(^1P)$		51.72	50.57	1.15
$2p^4(^1D)3s(^2D)5p(^1P)$		52.25	51.28	0.97
$2p^4(^1D)3s(^2D)6p(^1P)$		52.50	51.56	0.94
$2p^4(^1S)3s(^2S)3p(^1P)$	(53.5)	54.08	52.61	1.47
$2p^4(^1S)3s(^2S)4p(^1P)$		55.65	54.36	1.19
$2p^4(^1S)3s(^2S)5p(^1P)$		56.15	55.00	1.15
Ionic states				
$2s^1 2p^6(^2S_{1/2})$	47.90	48.90	48.48	0.42
$2p^4(^3P)3s(^4P)$	48.34	49.23	48.77	0.54
$2p^4(^3P)3s(^2P)$		49.96	49.37	0.61
$2p^4(^1D)3s(^2D)$	51.74	52.57	52.12	0.45
$2p^4(^3P)3p(^4D)$	(52.13)		52.49	
$2p^4(^3P)3p(^2D)$	52.33	53.31	52.71	0.60
$2p^4(^3P)3p(^2P)$	52.87	53.85	53.09	0.76
$2p^4(^1D)3p(^2F)$	55.23	56.31	55.58	0.73
$2p^4(^1D)3p(^2P)$	55.48	56.61	55.83	0.78
$2p^4(^3P)3d(^{4,2}D)$	55.82	56.90	56.33	0.57
$2p^4(^3P)4s(^2P)$	56.71	57.64	56.74	0.90
$2p^4(^3P)4p(^{4,2}S)/(^2D)$		58.28	57.85	0.43
$2p^4(^3P)4p(^2P)$		58.43	58.04	0.39
$2p^4(^3P)4p(^4D)$	(57.95)	(59.13)		
$2p^4(^1S)3p(^2S)$		60.55	59.50	1.05

Inspection of the energy values in Table 1 reveals interesting differences. Excitation energies of surface excitons are smaller than those of the corresponding bulk states, and surface as well as bulk exciton energies are always larger than the gas phase values, although this difference is small for some surface states. The condensation shifts are largest for the series members with the lowest principal quantum numbers. For identical quantum numbers, the differences tend to be larger for the doubly compared to the singly excited states. All of these findings underline the importance of the caging effect that prevails for low principal quantum numbers and for the bulk compared to the surface states (see above).

For the continuum states the situation is less "monotonic". Here we find for practically all $[2p^2]nl$ satellite lines of our study the ionization potential of the isolated atom between that of the surface (lower) and that of the bulk (higher). The lowering at the surface is clearly due to polarization screening of the electron hole interaction; the blue shift of the bulk states however is caused by the negative electron affinity, which requires extra energy to create a free electron inside the solid. In summary, all Rydberg series are compressed with respect to the gas phase, however those pertaining to bulk states less efficiently that their surface analogues (Table 1).

These differences of the condensation shifts for neutral and ionic states enable new decay scenarios that explain the remarkably deviating line profiles of the [2*s*]3*p* and [2*s*]4*p*,5*p* bulk excitons (Fig. 2,*a*). [2*s*]3*p* shows a bipolar Fano profile, whereas the higher members of the series exhibit nearly symmetric maxima. The surface series, on the other hand, shows Fano profiles for all principal quantum numbers. This anomaly of the higher bulk states indicates the contribution of additional decay routes, which result from the bulk-to-surface shift of the ionization potentials. The energies of all but the lowest [2*s*]*np* states lie above the outer [2*s*] ionization potential, and decay of the [2*s*]*np* bulk excitons into the [2*s*] continuum *at the surface* is possible for $n > 3$. This is best seen in Fig. 3 that displays the low-energy side of an electron distribution similar to that shown in Fig. 1.

The [2*s*] CIS trace shows well discernible maxima at the energy positions of the [2*s*]4*p*, [2*s*]5*p* and [2*s*]6*p* states. Surprisingly, decay of bulk excitons into ionic surface states is also possible for doubly excited excitons, best seen for the $(^1D)3s(^2D)np$ series. The high intensity of the $(^3P)3p(^2P)$ emission on top of the conduction band is caused by autoionization of the $(^1S)3s(^2S)3p$ exciton into this continuum, a process that is energetically forbidden in the gas phase (see the energy values in Table 1).

We finally focus on dynamics limitations of the decay of bulk excitons by ionization at the surface; obviously, these excitons have to migrate to the surface before they decay, i.e., some mobility is required. One could argue that the large, spatially extended excitonic wave functions of large quantum numbers have some density of states at the surface anyway, however a look at the 2D spectrum for the [1*s*] threshold region tells us that for the immobile and short lived inner core states such a process does not occur (Fig. 4, bottom). For the mobile, delocalized outer valence excitons [6], however, ionization of higher bulk excitons at the surface is very important; the corresponding maxima are as large as the peak corresponding to electron emission

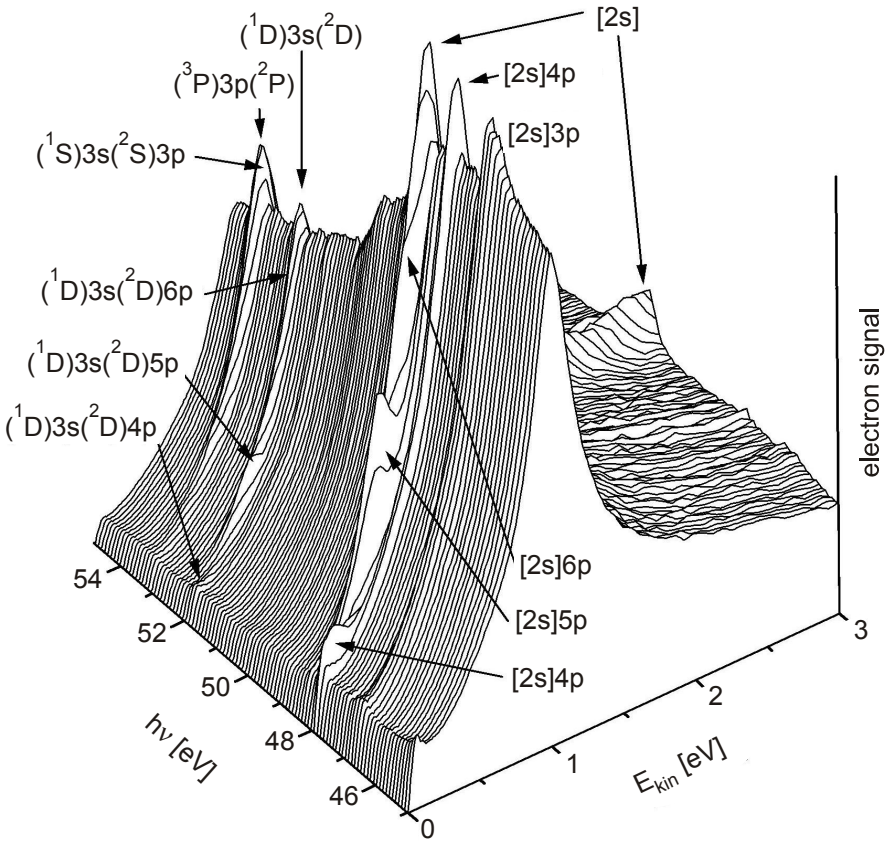

Fig. 3. Neutral bulk excitations (bulk excitons) decaying into ionic surface states cause maxima in photoelectron emission at kinetic energies between E_{vac} and E_{cb}. Such processes are observed for the higher members of the [2*s*]*np* series as well as (less pronounced) for doubly excited states derived from 2*p* levels. The strong enhancement of the $(^3P)3p(^2P)$ signal at E_{cb} is due to autoionization of the neutral $(^1S)3s(^2S)$ 3*p* state.

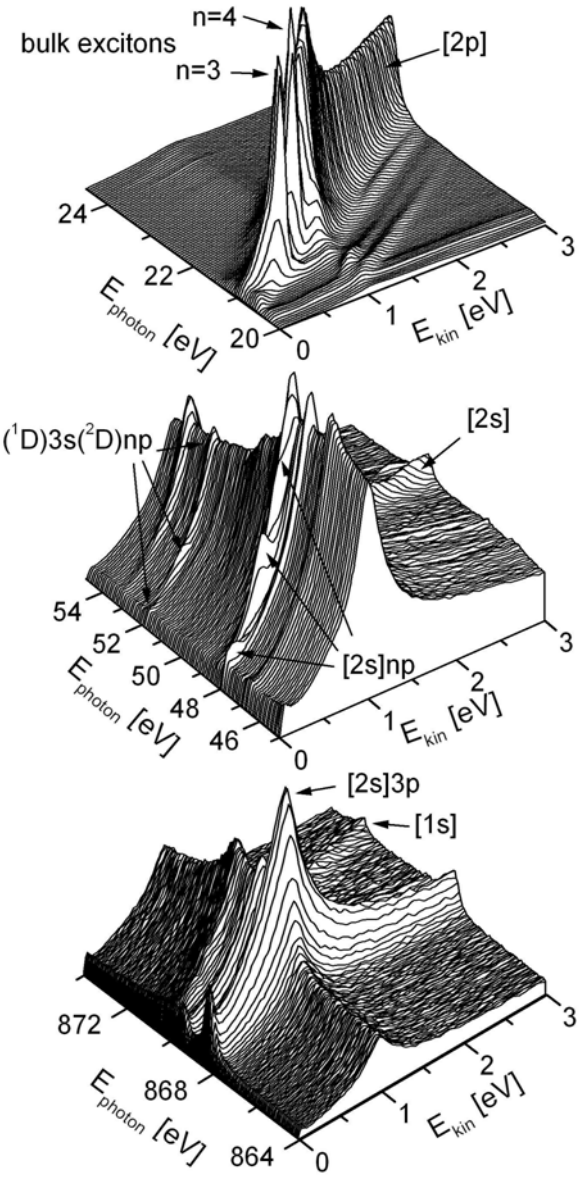

Fig. 4. The tendency of bulk excitons to ionize at the surface decreases from outer valence excitons (top) to double excitations of outer valence levels (middle panel). Excitons of inner valence levels are an intermediate case (middle). For core excitons this effect is absent (lower panel).

from the band bottom (Fig. 4, top, and Ref. 7). Obviously, mobility of the excitation is required for this decay process. Accordingly, it is strong for the delocalized [2*p*]*ns* valence excitons and absent for the [1*s*]*np* core excitons. From the results in Figs. 3, 4 we can conclude that the inner valence [2*s*]*np* excitons are an intermediate case with reduced mobility. Surprisingly, the doubly excited states also exhibit at least a limited mobility, larger than that of the inner shell excitations, but much smaller than that of the outer valence excitons, simply because the two holes must move simultaneously. This is a nice demonstration of the reduced mobility and efficient localization of core and double ionizations at distinct bonds, a property that makes these kinds of excitations so important for bond breaking reactions by electronic stimulation [25].

In summary, we have shown that 2D electron spectroscopy can supply plenty of information on the electronic properties of thin film sample, even if they are electrically insulating and very sensitive to radiation defects like damage formation and charging. The data obtained comprise not only precise energy values for surface and bulk states but also valuable information upon their mobility and decay routes.

Acknowlegments

We thank D. Menzel for fruitful discussions, and P. Averkamp and the staff of BESSY for help during the experiments. Support by the Helmholtz Zentrum Berlin is gratefully acknowledged.

1. N. Schwentner, E.-E. Koch, and J. Jortner, *Electronic Excitations in Condensed Rare Gas Solids*, Springer Tracts in Modern Physics **107**, Springer, Berlin (1985), and references therein.
2. Yi-guang He, Xiu-zhang Tang, and Yi-kang Pu, *Physica* **B405**, 4335 (2010), and references therein.
3. N.R. Werthamer, *Am. J. Phys.* **37**, 763 (1969).
4. K. Codling, R.P. Madden, and D.L. Ederer, *Phys. Rev.* **155**, 26 (1967).
5. see, e.g., S.E. Canton, A.A. Wills, T.W. Gorczyca, E. Sokell, J.D. Bozek, G. Turri, M. Wiedenhoeft, X. Feng, and N. Berrah, *J. Phys.* **B36**, L181 (2003).
6. G. Zimmerer, in: *Excited State Spectroscopy in Solids*, North Holland, Amsterdam (1987), p. 37, and references therein.
7. B. Kassühlke, R. Romberg, P. Averkamp, and P. Feulner, *J. Low. Temp. Phys.* **111**, 723 (1998).
8. R. Romberg, B. Kassühlke, P. Wiethoff, D. Menzel, and P. Feulner, *Chem. Phys.* **289**, 69 (2003), and references therein.
9. P. Wiethoff, B. Kassühlke, D. Menzel, and P. Feulner, *Fiz. Nizk. Temp.* **29**, 351 (2003) [*Low Temp. Phys*. **29**, 266 (2003)].
10. R. Haensel, G. Keitel, N. Kosuch, U. Nielsen, and P. Schreiber, *J. Phys. (Paris), Colloq*. **32**, C4-236 (1971).
11. H. Schlichting and D. Menzel, *Surf. Science* **272**, 27 (1992); *ibid.* **285**, 209 (1993).
12. P. Wiethoff, H.-U. Ehrke, D. Menzel, and P. Feulner, *Phys. Rev. Lett.* **74**, 3792 (1995).
13. B. Kassühlke, P. Averkamp, S. Frigo, P. Feulner, and W. Berthold, *Phys. Rev.* **B55**, 10854 (1997).
14. P. Wiethoff, H.-U. Ehrke, B. Kassühlke, C. Keller, W. Wurth, D. Menzel, and. P. Feulner, *Phys. Rev.* **B55**, 9387 (1997).
15. P. Feulner, P. Averkamp, and B. Kassühlke, *Appl. Phys.* **A67**, 657 (1998).
16. B. Kassühlke, *PhD-thesis*, TU-Müchen (1998).
17. N.C. Bacalis, D.A. Papaconstantopoulos, and W.E. Picket, *Phys. Rev.* **B38**, 6218 (1988).
18. J. Stöhr, *NEXAFS Spectroscopy*, Springer, Berlin (1992).

19. see, e.g., C.T. Reimann, W.L. Brown, and R.E. Johnson, *Phys. Rev.* **B37**, 1455 (1988), for typical fluorescence yields from rare-gas layers on metal substrates as a function of film thickness.
20. U. Fano, *Phys. Rev.* **124**, 1866 (1961); and references therein.
21. J.L. Campbell and T. Papp, *Atomic Data Nuclear Data Tables* **77**, 1 (2001).
22. J.-P. Gauyacq and A.K. Kazansky, *Chem. Physics* **327**, 300 (2006).
23. A.A. Wills, A.A. Cafolla, A. Svensson, and J. Comer, *J. Phys.* **B23**, 2013 (1990).
24. P.A. Heimann, U. Becker, H.G. Kerkhoff, B. Langer, D. Szostak, R. Wehlitz, D.W. Lindle, T.A. Ferrett, and D.A. Shirley, *Phys. Rev.* **A34**, 3782 (1986).
25. P. Feulner and D. Menzel, in: *Laser Spectroscopy and Photochemistry on Metal Surfaces, Part II*, World Scientific, Singapore (1995), chapt. 16, and references therein.